A SIMULATION OF THE PERFECTLY MATCHED LAYER IN THE 3-D CASE

Ioana SĂRĂCUȚ Victor POPESCU Dan Ovidiu MICU
Technical University of Cluj-Napoca,
G.Baritiu Street 26-28, Cluj-Napoca, phone 0264-401803
E-mails: Ioana.Saracut@bel.utcluj.ro , Victor.Popescu@bel.utcluj.ro , DanO.Micu@et.utcluj.ro

Abstract: The Perfectly Matched Layer (PML) technique, introduced by J. P. Berenger in 1994, is used for solving unbounded space problems. In this paper we implemented in Matlab a three dimensional Finite-Difference Time-Domain coordinate space surrounded by PML. First we evaluated the performances of the PML when a plane wave having a Gaussian pulse profile propagates. Then a dipole antenna is simulated in the same computational space and some simulation results, including the radiation pattern, are presented.

Key words: *Finite-Difference Time-Domain, Perfectly Matched Layer, electromagnetic field, dipole antenna.*

I. INTRODUCTION

The *Finite-Difference Time-Domain* (FDTD) method is a volume discretization technique introduced by Kane S. Yee in 1966. Yee proposed the time and space discretization of the differential form of Maxwell's equations, using central differences. The electric and magnetic fields are then evaluated at alternate half-time steps on a Cartesian grid [1].

The application of the FDTD method in many problems in open domains requires the truncation of the space, in order to simulate the propagation of electromagnetic energy out of the computational space and without introducing significant artifacts into the computation.

The *Perfectly Matched Layer* (PML) technique was proposed by J.P. Berenger in 1994, for solving unbounded electromagnetic problems with the FDTD method. The PML is a layer of artificial absorbing material, which is placed adjacent to the edges of the grid. Berenger showed that this special absorbing medium is constructed so that waves do not reflect at the interface [4]. As a wave enters the PML, it is attenuated by the absorption and decays exponentially; even if it reflects off the boundary, the inverse wave is exponentially tiny.

Berenger verified the accuracy of the PML technique in 2-D FDTD coordinate space and Daniel F. Katz extended the same technique for a 3-D FDTD grid [7].

Section II of this paper presents the theory of the 3-D discretization and the modeling of the PML. In Section III we simulated the propagation of a plane electromagnetic wave in a 3-D space bounded by PML and the simulation results are presented. Then we simulated the radiation of a dipole antenna. Finally, Section IV gives some concluding remarks.

II. THE 3-D MODEL OF THE UNBOUNDED SPACE

A 3-D FDTD simulated space consists of a multiplicity of cubic cells, called *Yee cells* [1]. In a Yee cell the electric field components are positioned in the middle of the edges of the cube, and the magnetic field components are positioned in the center of the faces. A field component is a function of space and time and is denoted as $F^n(i, j, k)$, where i, j, k are the spatial coordinate and n is the time coordinate.

A 2-D discretized structure consists of squares instead of cubes and some of the field components are defined in the corners of these squares [1, 9, 10]. Their spatial indices are integer, while the other components have fractional indices.

In the 3-D case, there isn't any filed component defined in the corners of the cube, therefore all the components will have fractional spatial indices. *Figure 1* illustrates such a Yee cell, where we place, as an example, a few of the ***E***-field and ***H***-field components.

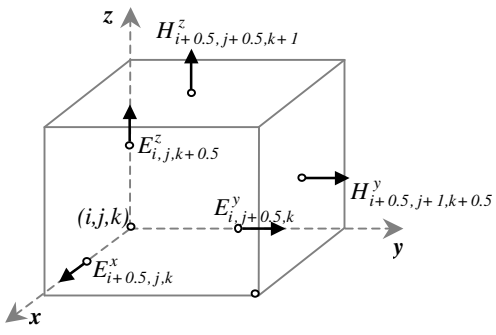

Figure 1. A Yee cell with fractional spatial indices.

Manuscript received April 23, 2010; revised June 14, 2010

The Matlab program requires that the indices of the matrices are integers. Hence, even if the fractional indices for time and space used by Yee are very suggestive for understanding the algorithm, it is not suitable for the practical implementation. In our spatial discretization, integer indices are used instead of fractional indices, following the next principle: with the notations used in *Figure 2*, the components with indices (*i*, *j*, *k*) are:

- the ***E***-components that are closer to the node (*i*, *j*, *k*);
- the ***H***-components that are defined on the related faces of the cube.

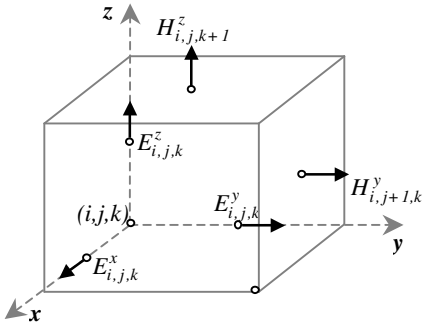

Figure 2. A Yee cell with integer spatial indices.

The fractional time indices suggest that the field components that are in different locations are calculated at different moments (the necessary time for the wave to propagate). We used integer indices for time too, making sure that in one iteration first *all* the ***E*** components are calculated then *all* the ***H*** components (or vice versa).

Consider the propagation of a plane electromagnetic wave, in a *3*-D Cartesian coordinates, along the *y* axis. Consider the most general medium, having an electric conductivity s_e and a magnetic conductivity s_m. For implementation, Maxwell's equations were replaced by a system of finite-difference equations on the mesh. For example, Maxwell's equations that give the *x*-components of ***E*** and ***H*** are:

$$e_0 \frac{\partial E_x}{\partial t} + s_e E_x = \frac{\partial H_z}{\partial y} - \frac{\partial H_y}{\partial z} \tag{1}$$

$$m_0 \frac{\partial H_x}{\partial t} + s_m H_x = \frac{\partial E_y}{\partial z} - \frac{\partial E_z}{\partial y} \tag{2}$$

where e_0 and m_0 are the permittivity and permeability of the vacuum. It has been shown [6] that if

$$\frac{s_e}{e_0} = \frac{s_m}{m_0} \tag{3}$$

then no reflection occurs when a plane wave propagates normally across a vacuum-medium interface.

The finite-difference approximation for the *x*-components of ***E*** and ***H*** are:

$$\begin{aligned} E_x^{n+1}(i,j,k) &= a_e \cdot E_x^n(i,j,k) - \\ &- b_e \cdot \left[H_y^n(i,j,k) - H_y^n(i,j,k-1) \right] + \\ &+ b_e \cdot \left[H_z^n(i,j,k) - H_z^n(i,j-1,k) \right] \end{aligned} \tag{4}$$

$$\begin{aligned} H_x^{n+1}(i,j,k) &= a_m \cdot H_x^n(i,j,k) + \\ &+ b_m \cdot \left[E_y^n(i,j,k+1) - E_y^n(i,j,k) \right] - \\ &- b_m \cdot \left[E_z^n(i,j+1,k) - E_z^n(i,j,k) \right] \end{aligned} \tag{5}$$

where a_e, b_e, a_m, b_m are absorbing coefficients.

Similar finite-difference approximations for the *y*- and *z*-components can easily be derived.

Absorption in PML

In vacuum $a_e = a_m = 1$, thus the electromagnetic wave propagates lossless. In the PML, these two coefficients progressively decrease with the thickness of the layer. This decreasing ensures the impedance matching at the interface and a progressive absorption of the wave.

We considered the absorption in PML as a polynomial function of the depth (*y*) in PML :

$$a(y) = 1 - \frac{1 - a_{min}}{g^n} \cdot y^n \tag{6}$$

where $0 < y < g$, *g* is the thickness of the PML, a_{min} is the minimum value of the attenuation in PML ($0 < a_{min} < 1$) and *n* is the order of the polynomial variation. The variation of the absorption is shown in *Figure 3*.

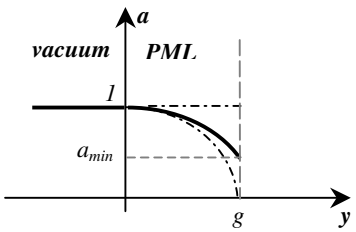

Figure 3. The variation of the absorption in the PML

As a result, the absorption in PML depends on two parameters: *g* and a_{min}, about which we make the following remarks:

- the thickness *g* must be as small as possible, in order to reduce the computations;
- if $a_{min} = 1$, the wave propagates lossless and there are reflections from the external boundary of the PML, as if the boundary was a conductor.
- if $a_{min} = 0$, it is possible that a too steep variation of the attenuation produces reflections too, especially when *g* also is small.

The reflection coefficient

Consider two different homogeneous media and a plane wave which travels through medium *1*. When meeting medium *2*, a part of the wave is reflected back while the rest of it travels through medium *2*. The reflected wave (U_r) is related to the incident wave (U_i) by the relation: $U_r = K_r \times U_i$, where K_r is the reflection coefficient.

When the two media are homogeneous, the surface of separation is sharp and the two waves have different amplitudes but the same duration. In this case, the reflection coefficient is calculated as the ratio of the amplitudes of the reflected and incident waves:

$$K_r = \frac{U_r}{U_i} \tag{7}$$

The phenomenon is different if the medium *2* is non-homogeneous (as is the PML). As the wave impedance increases in depth, the reflected wave can be seen as a superposition of partial reflected waves. Their delays increase as the reflection occurs in a deeper layer. Considering the same incident wave as before, the reflected wave has now a longer duration. In this case, K_r will be computed as the ratio of the waves' energies:

$$K_r = \sqrt{\frac{W_r}{W_i}} \tag{8}$$

PML in 3-D

A 3-D model of a FDTD domain surrounded by PML can be considered as a box (see *Figure 4*): the inside represents the isotropic medium, while the walls are the absorbent layers. There are *3* types of PML with the same attenuation characteristic, but having different properties:

(a) the faces absorb in one direction (which is the normal to the face);
(b) the edges absorb in two directions;
(c) the corners absorb in three directions.

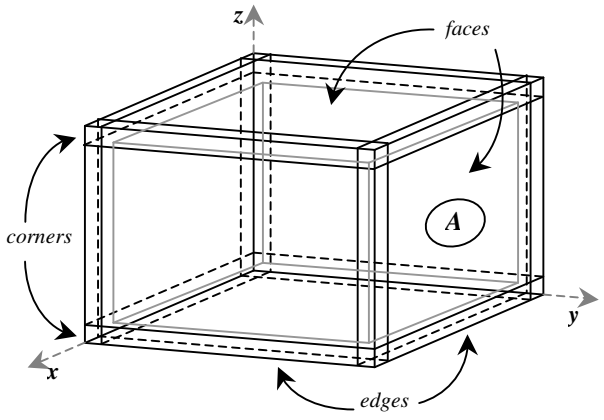

Figure 4. The 3-D model of the computational domain

In the PML, the components of the field are split into sub-components, depending on the direction of propagation. For example, on the face *A*, the tangential components are split as follows:

$$\begin{aligned} E_x &= E_{xy} + E_{xz} & H_x &= H_{xy} + H_{xz} \\ E_y &= E_y & H_y &= H_y \\ E_z &= E_{zx} + E_{zy} & H_z &= H_{zx} + H_{zy} \end{aligned} \tag{9}$$

In this case, the pairs of components that are attenuated are: (E_{xz}, H_{zx}), (E_{zx}, H_{xz}), while the pairs of components that propagate without attenuation are: (E_{xy}, H_y), (E_{zy}, H_y), (E_y, H_{zy}) and (E_y, H_{xy}).

III. SIMULATION RESULTS

We simulated in Matlab a 3-D free-space computational domain surrounded on all sides by PML. The FDTD space grid was chosen so that the electromagnetic field doesn't change significantly over one increment. For computational stability, it is necessary that [1]:

$$\sqrt{(\Delta x)^2 + (\Delta y)^2 + (\Delta z)^2} > c \cdot \Delta t = \Delta \tau \tag{10}$$

where Δx, Δy and Δz are the dimensions of a cell, c is the speed of light in vacuum and Δt is the time increment.

We considered $\Delta x = \Delta y = \Delta z = 2 \cdot \Delta \tau$. In this way, the time step of iteration is the necessary time for the wave to travel half of a cell size, which is the distance between the points where the ***E***-components and the ***H***-components are computed. The dimensions of the simulated space were set as follows:

- the cell size: $0.09 \times 0.09 \times 0.09$ *m*;
- the FDTD grid (without PML): $40 \times 100 \times 40$ cells;

The results were giving after *500* time steps, with the time increment *150 ps*.

The plane wave

As an excitation we considered a plane wave, with its profile being a Gaussian pulse, having the amplitude of *1V* and the duration of *8 ns* (see *Figure 5*).

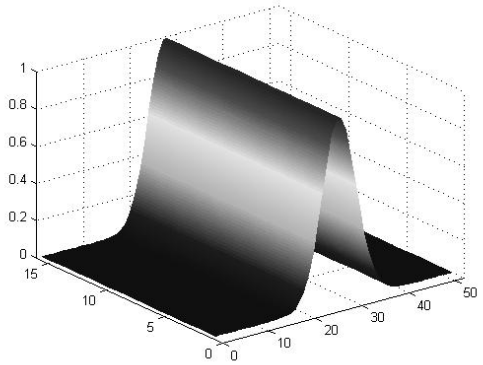

Figure 5. The incident plane wave

The source was placed in the computational zone, in the middle of the face *x0z*, two cells away from the PML.

In order to verify if the wave is plane, we calculated its energy in the middle of the isotropic space and in the PML. Equal values resulted, which demonstrates that the energy is conserved, thus there isn't any deformation at the microscopic level.

For comparison, *Figure 6* shows the Gaussian pulse used in our simulations and the pulse used by Berenger. The vertical dashed line marks the surface the separation between the isotropic medium (on the left) and the PML (on the right). For a better view, the areas in the grey rectangles were enlarged and illustrated in *Figure 7*.

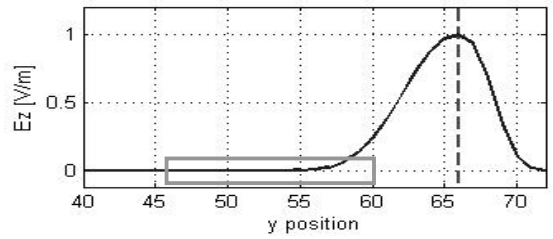

(a)

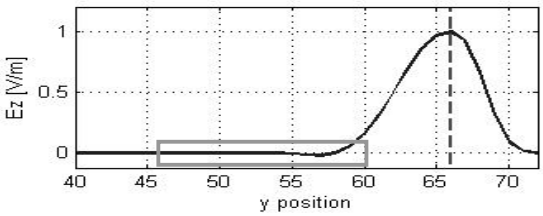

(b)

Figure 6. (a) The Gaussian pulse; (b) The Berenger's pulse (Note: the areas in the grey rectangles are pictured in higher resolution in Figure 7)

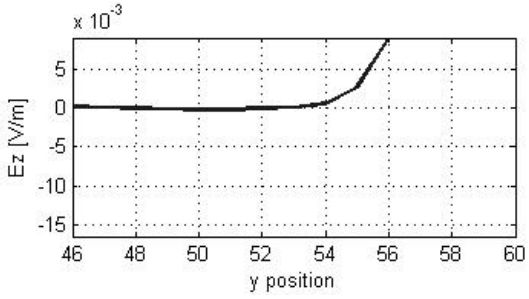

(a)

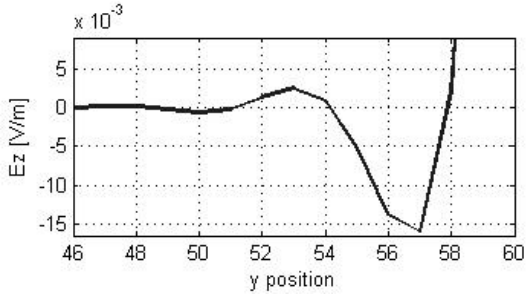

(b)

Figure 7 (detailed) (a) The Gaussian pulse; (b) The Berenger's pulse

It can be seen that between the positions $y = 52$ and $y = 59$ the Gaussian pulse used in our simulations has a smooth increasing, while Berenger's pulse oscillates.

Figure 8 shows the E_z field as a function of *y* position (which is the direction of propagation), for $g = 6$ cells, $a_{min} = 0.1$ and $n = 2$ (the absorption in PML has a quadratic dependence on depth).

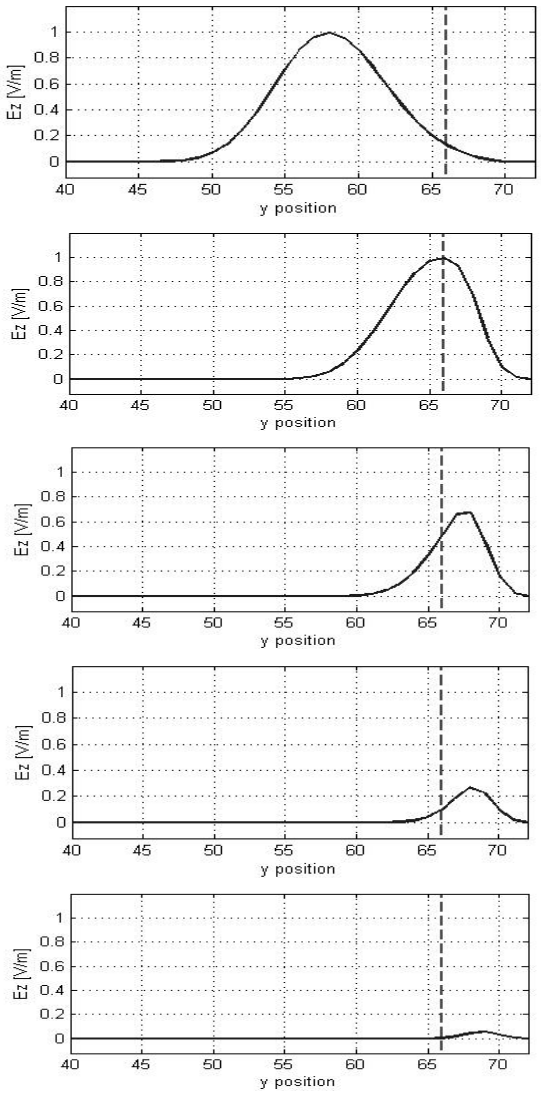

Figure 8. The E_z field as a function of the position on y axis

It can be seen how the PML affect the incident wave: its amplitude decreases as the wave travels through the PML. The reflection coefficient in this case resulted *0.051 %* .

We also studied the consequences of varying a_{min} for a fixed value of PML's thickness *g*. *Figure 9* compares the reflection coefficient for $g = 6$, *8* and *10* cells respectively, in the case when the attenuation has a

quadratic variation ($n = 2$) and a_{min} ranges from *0* to *0.7*. *Figure 10* compares the reflection coefficient for the same values for g and a_{min} as before, but for a cubic variation of the attenuation ($n = 3$).

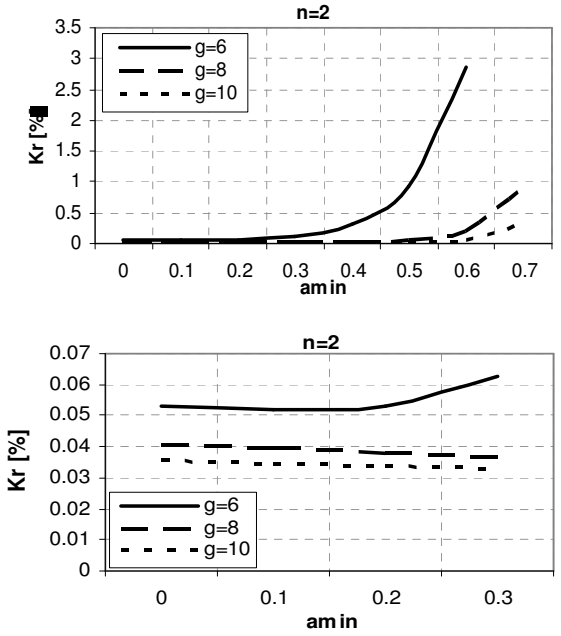

Figure 9. The reflection coefficient as a function of a_{min} for quadratic dependence

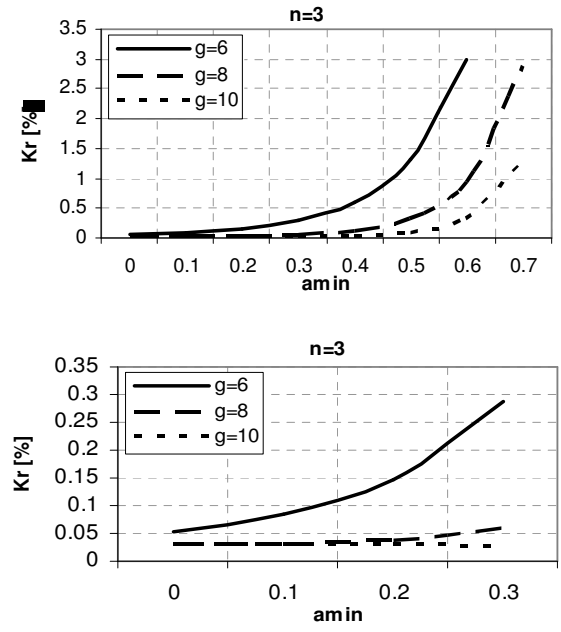

Figure 10. The reflection coefficient as a function of a_{min} for cubic dependence

In the upper part of *Figure 9* it can be seen the increasing of the reflection coefficient with increasing of a_{min}. But when looking at the lower part of the figure, one can notice that the reflection coefficient decreases slightly (for $0 < a_{min} \le 0.3$ when $g = 8$ and $g = 10$; for $0 < a_{min} \le 0.15$ when $g = 6$). Also *Figure 10* (the lower graph) shows that for small values of a_{min} the reflection coefficient increases only for $g = 8$ and $g = 10$. As expected, if the variation of the attenuation is too steep, then reflections of small amplitudes occur. However, the reflection coefficient in this case has very low values: between *0.03%* and *0.06%* for $0 < a_{min} \le 0.3$.

Radiation of a dipole antenna

We simulated a half-wavelength dipole antenna, situated in a plane normal to *x* axis, parallel to the *z* axis, at one cell distance from the PML and positioned symmetrically in respect to the *xy* plane, as shown in *Figure 11*. Each of the two elements AB and CD has a *10* FDTD cells length and the distance between them is *2* cells.

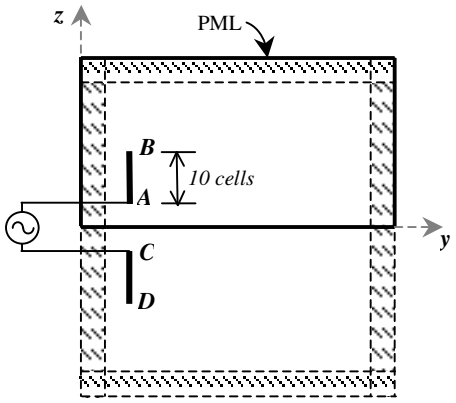

Figure 11. The dipole antenna situated in the computational domain

Due to the symmetry of the problem, we used the method of images, in order to reduce the calculations: the plane *xy* is equipotential, therefore we simulated only half of the computational domain (which is the outlined rectangle in *Figure 11*) and we considered *xy* as being conductor. In this case the field distribution between the conductor and the element AB is the same as between AB and CD.

Figure 12 shows the *Hx* field radiated by the antenna, at the time step *349*. For better understanding, we also placed in the figure the element AB of the dipole. The rectangle (with continuous line) represents the median plane of the antenna, considered as conductor in the method of images. It can be seen that the oscillations along *y*-axis have maximum amplitude (the radiation is maximum). Along *z*-axis, which would correspond to the radiation directly overhead the antenna, there is very little power transmitted (on the *z*-axis, the field varies only along the antenna and it is zero in the rest of the axis). For the rest of the outline, one can notice that the wave is attenuated in the PML.

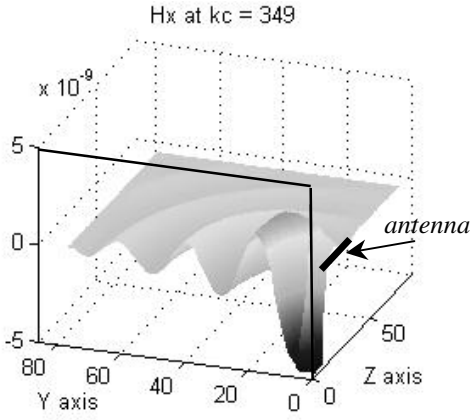

Figure 12. The Hx field radiated by the dipole antenna (only half of the plane was simulated)

Figure 13 illustrates the two-dimensional radiation pattern of the dipole antenna (with continuous line), for a radius $r = 68$ cells. The radiation pattern of an infinitesimal dipole is also included for comparison (with dashed line).

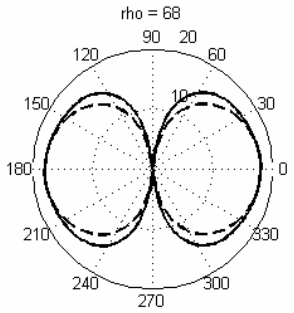

Figure 13. The radiation pattern of the dipole antenna (with continuous line)

The sinusoidal current distribution along the antenna was imposed. The elementary currents cause the movement of the electric charges; the charge accumulated in the corners of the FDTD cells results from the difference of the adjacent currents.

In order to match the propagation speed in antenna to the propagation speed in the computational domain, the dipole was discretized at double the resolution of the computational space. The field right near the antenna was calculated as follows: (1) the charges produce the E_x and E_y field (the potential field); (2) the elementary currents generate the H_x and H_y field (the solenoidal field). These field components realize the interface between the dipole antenna (the electric circuit) and the exterior medium.

We evaluated the radiated powers on the sphere of radius r by interpolation. The energy is given by the Poynting vector: $\boldsymbol{S} = \boldsymbol{E}' \boldsymbol{H}$, but the $\boldsymbol{E}$- and the $\boldsymbol{H}$-components are calculated in different locations on the FDTD grid, hence we used the interpolation to calculate the values of the field components in the same point on the sphere.

IV. CONCLUSIONS

In this paper, we simulated in Matlab the propagation of the electromagnetic field in a 3-D space surrounded by an artificially layer called PML. First we show that the Gaussian pulse conserve its shape even at very low resolution. We show that theory predictions for volume reflection agree with the simulation results. The volume reflection phenomenon does occur, but the PML attenuates very efficiently the incident wave so that the minimum value of the attenuation can be chosen zero.

We also simulated the radiation of a dipole antenna. When the computational zone is symmetric, the method of images can be used in the 3-D FDTD models with PML. We specify that the electromagnetic phenomena in the antenna were partially simulated. This topic will be addressed in further papers. We intend to realize a more rigorous model of the phenomena that occur inside and near the dipole antenna.

REFERENCES

[1] K.S.Yee, "*Numerical Solution of Initial Boundary Value Problems Involving Maxwell's Equations in Isotropic Media*", IEEE Transactions on Antennas and Propagation, vol.AP-14, no.8, pp.302-307, May 1966.

[2] W.V.Andrew *et al*., "*A Comparison of the Berenger Perfectly Matched Layer and the Lindman Higher-Order ABC's for the FDTD Method*", IEEE Microwave and Guided Wave Letters, vol.5, no.6, pp.192-194, June 1995.

[3] C.A. Balanis, "*Antenna Theory. Analysis and Design – 2nd ed.* ", John Wiley & Sons, Inc., New York, 1997.

[4] J.P.Berenger, "*A Perfectly Matched Layer for the Absorption of Electromagnetic waves*", J.Computational Physics, vol.114, pp.185-200, Oct. 1994.

[5] J.P.Berenger, "*Evanescent Waves in PML's: Origin of the Numerical Refletion in Wave-Structure Interaction Problems*", IEEE APS, vol.47, pp.1497-1503, Oct. 1999.

[6] J.P.Berenger, "*Numerical Reflections from FDTD-PML's: A Comparison of the Split PML with the Unsplit and CFSPMLs*", IEEE APS, vol. 50, pp.258-265, March 2002.

[7] D.S. Katz, T.T.Thiele, A. Taflove, "*Validation and Extension to Three Dimensions of the Berenger PML Absorbing Boundary Condition for FD-TD Meshes*", IEEE Microwave and Guided Wave Letters, vol.4, no.8, pp.268-270, Aug. 1994.

[8] W.C.Chew, W.H.Weedon, "*A 3D Perfectly Matched Medium from Modified Maxwell's Equations with Stretched Coordinates*", Microwave and Optical Technology Letters, vol. 7, no. 13, pp. 599–604, September 1994.

[9] R.L.Higdon, "*Numerical Absorbing Boundary Conditions for the Wave Equation*", Mathematics of Computation, vol. 49, pp. 65-90, 1987.

[10] E.L.Lindman, "*Free Space Boundary Conditions of the Time Dependent Wave Equation*", J.Computational Phys., vol.18, pp.66-78, 1975.

[11] P.A.Tirkas, C.A. Balanis, "*Higher-Order Absorbing Boundary Conditions in FDTD Method*", IEEE Transactions on Antennas and Propagation, vol.40, no.10, pp.1215-1222, October 1992.